Geological Magazine

www.cambridge.org/geo

Rapid Communication

Cite this article: Parnell J, Brolly C, and Boyce AJ (2021) Graphite from Palaeoproterozoic enhanced carbon burial, and its metallogenic legacy. *Geological Magazine* **158**: 1711–1718. https://doi.org/10.1017/S0016756821000583

Received: 14 December 2020
Revised: 14 May 2021
Accepted: 26 May 2021
First published online: 13 July 2021

Keywords:
Precambrian; Proterozoic; graphite; mineralization; carbon isotopes

Author for correspondence: John Parnell, Email: J.Parnell@abdn.ac.uk

CAMBRIDGE UNIVERSITY PRESS

Graphite from Palaeoproterozoic enhanced carbon burial, and its metallogenic legacy

John Parnell[1], Connor Brolly[1] and Adrian J. Boyce[2]

[1]School of Geosciences, University of Aberdeen, Aberdeen AB24 3UE, UK and [2]Scottish Universities Environmental Research Council (SUERC), East Kilbride, Glasgow G75 0QF, UK

Abstract

The episode of widespread organic carbon deposition marked by peak black shale sedimentation during the Palaeoproterozoic is also reflected in exceptionally abundant graphite deposits of this age. Worldwide anoxic/euxinic sediments were preserved as a deep crustal reservoir of both organic carbon, and sulphur in accompanying pyrite, both commonly >1 wt %. The carbon- and sulphur-rich Palaeoproterozoic crust interacted with mafic magma to cause Ni–Co–Cu–PGE mineralization over the next billion years, and much uranium currently produced is from Mesoproterozoic deposits nucleated upon older Palaeoproterozoic graphite. Palaeoproterozoic carbon deposition has thus left a unique legacy of both graphite deposits and long-term ore deposition.

1. Introduction

The Palaeoproterozoic Lomagundi–Jatuli Event was a major anomaly in the global cycling of carbon which records a positive excursion in $\delta^{13}C$ composition in carbonates worldwide (Melezhik *et al.* 2007). This event was closely followed by the deposition of extensive black (carbon-rich) shales, the Shunga Event ~2.0 Ga, on several continents (Condie *et al.* 2001; Strauss *et al.* 2013; Martin *et al.* 2015). The abundance of carbon may reflect intense weathering of the continents following the Great Oxidation Event, and high productivity in the nutrient-rich oceans (Melezhik *et al.* 2013). The identification of this episode as the peak of black shale sedimentation in the Precambrian, from 2.0 to 1.85 Ga (Condie *et al.* 2001), is based on data from Australia (57 %), North America (37 %) and Russia (6 %). New exploration for graphite deposits, required for industrial processes, batteries and possibly manufacture of graphene, has drawn attention to many additional successions of Palaeoproterozoic black shale, now metamorphosed to graphitic metasediments, and the unique nature of this carbon burial episode.

The record of graphite as a measure of Palaeoproterozoic carbon burial is expressed here as (i) a review of the depositional ages of the biggest graphite deposits, (ii) a compilation of carbon/sulphur elemental datasets for graphitic metasediments and (iii) a review of carbon isotope compositions of Palaeoproterozoic graphite. Combined, the data will confirm if the Palaeoproterozoic was a period of anomalous carbon burial, if the carbon was derived from sedimentary organic matter rather than carbonic fluids during metamorphism, and if the carbon caused burial of sulphur as in younger sediments.

2. Methods

Stable carbon isotope analysis was conducted at SUERC on 20 graphitic samples digested in 10 % HCl overnight to remove trace carbonate. Samples were analysed by standard closed-tube combustion method by reaction *in vacuo* with 2 g of wire form CuO at 800 °C overnight. Data are reported in per mil (‰) using the δ notation versus Vienna Pee Dee Belemnite (V-PDB). Repeat analysis of laboratory standard gave $\delta^{13}C$ reproducibility around ±0.2 ‰ (1 s). Other isotopic data were collated from cited literature. Total organic carbon (TOC) and S contents were measured using a LECO CS225 elemental analyser at the University of Aberdeen, with standards 501-024 (Leco Instruments, instrument uncertainty ±0.05 % C, ±0.002 % S) and BCS-CRM 362. Data are reported on a carbon/sulphur cross-plot, relative to the modern marine composition (Berner & Raiswell, 1983). The datasets reported are for rock units with TOC levels above 1 wt %, i.e. they are classified as black shales (TOC >0.5 wt %; Huyck, 1990). The repeatability, based on three repeats of CRMs and blanks, was consistently within 1 wt %. Collation of the world's largest graphite deposits was performed using a typical industry cut-off for exploitation of 8 wt % carbon (data file available from the authors). Tonnages of ore at major ore deposits were collated from cited literature. The long-term legacy of the Palaeoproterozoic graphitic rocks for mineralization that is important to global metal resources is demonstrated by reviews herein of nickel (+cobalt–copper–PGE (platinum-group

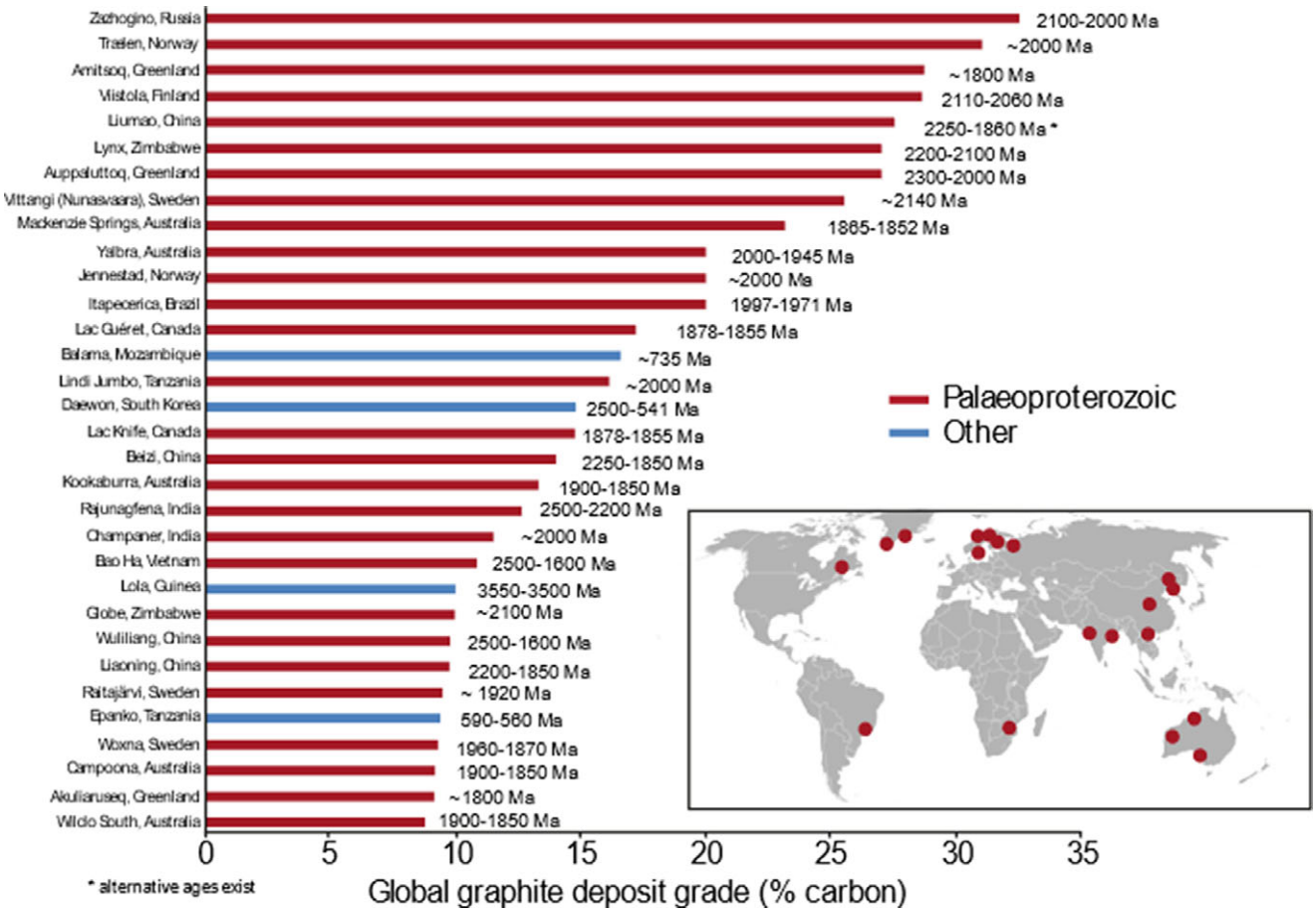

Fig. 1. (Colour online) World's richest graphite ore deposits. Deposits ranked by mean carbon content (wt %), collated from publicly available technical reports for exploration projects (Table S1, in the Supplementary Material available online at https://doi.org/10.1017/S0016756821000583). Data shown adopt a lower cut-off of 8 % carbon, commonly used in graphite exploration. Where clusters of several deposits occur together (e.g. at Balama), largest deposit is plotted. Palaeoproterozoic deposits highlighted and account for 28 of 33 richest deposits. Map shows global distribution of the richest graphite ores.

element)) mineralization, which occurs in mafic/ultramafic intrusions; and unconformity-related uranium mineralization.

3. Results

3.1. Anomalous Palaeoproterozoic carbon reservoir

Of the 33 richest graphite deposits in the world (minimum 8 wt % carbon), 28 of 33 (85 %) deposits are of Palaeoproterozoic age (Fig. 1; Table S1, in the Supplementary Material available online at https://doi.org/10.1017/S0016756821000583). Most of the deposits are dated to the range 2.1–1.85 Ga. Graphite deposits not dated to this interval are either Palaeoproterozoic but not so precisely dated, or Archaean. Hydrocarbon source rocks in younger successions are attributed excellent organic richness at mean contents above 4 wt % carbon, confirming the exceptional nature of the Palaeoproterozoic carbon accumulation. Younger episodes of high carbon accumulation, including in the late Neoproterozoic (Condie *et al.* 2001), were less extensive and thus had less opportunity to influence subsequent processes such as mineralization. The rich graphite deposits are predominantly vein-type, but there are many non-vein deposits of lower grade, and also younger less rich vein deposits (Robinson *et al.* 2017).

3.2. Sulphur contents of graphitic sediments

The cross-plot of organic carbon and sulphur (Fig. 2; Table S2, in the Supplementary Material available online at https://doi.org/10.1017/S0016756821000583) shows that in multiple datasets the S/C ratio is greater than the modern marine sediment value of *c.* 0.35. This is similarly reported in Palaeoproterozoic shales by Paiste *et al.* (2020). The direct implication is that the anomalously high carbon burial had the consequence of causing anomalously high sulphur sequestration in many Palaeoproterozoic successions. The carbon contents may be lower than originally deposited due to volatile loss during metamorphism (Raiswell & Berner, 1987), but correction for this would imply even richer carbonaceous deposits at the time of deposition.

Some Palaeoproterozoic black shales do not show a concomitant sulphur enrichment (e.g. de Putter *et al.* 2018), but most are sulphur-rich. While the shales are typically sulphur-rich, beds of mineable graphite are not sulphur-rich, and would not be commercially viable if they were (Lu & Forssberg, 2002; Chelgani *et al.* 2016).

3.3. Isotopic composition of Palaeoproterozoic graphite

As many of the graphite deposits were metamorphosed to amphibolite or granulite facies, it is feasible that the original sedimentary

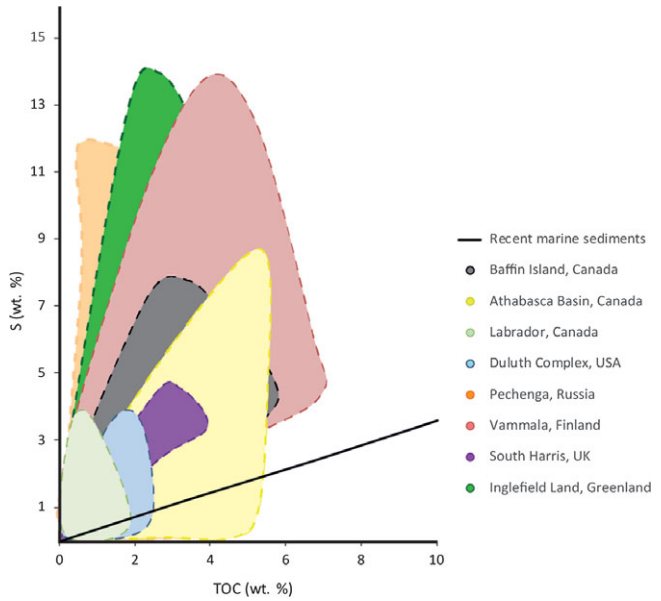

Fig. 2. (Colour online) Cross-plot of sulphur and organic carbon contents for Palaeoproterozoic country rocks for younger ore deposits and prospects. Reference line for recent marine sediments from Berner & Raiswell (1983). S/C ratios for these deposits are consistently higher than the line, reflecting extensive pyrite formation that would enhance mineralization during subsequent intrusion. Datasets (Table S2, in the Supplementary Material available online at https://doi.org/10.1017/S0016756821000583) from Andrews & Ripley (1989), Peltonen (1995), Melezhik *et al.* (1998), Ripley *et al.* (2002), Partin *et al.* (2015), Pascal *et al.* (2015) and this study (Greenland, UK).

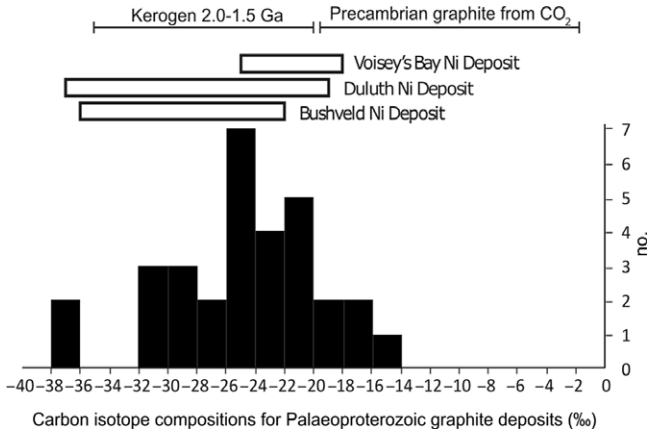

Fig. 3. Carbon isotopic compositions of Palaeoproterozoic graphite mines and prospective deposits, and three Ni ore deposits in Palaeoproterozoic rocks. Data from 15 countries, listed in Table S3, in the Supplementary Material available online at https://doi.org/10.1017/S0016756821000583. Data from graphite are similar to data from organic matter (kerogen) for period 2.0–1.5 Ga (Krissansen-Totton *et al.* 2015; Havig *et al.* 2017). Precambrian graphite precipitated from carbon dioxide has distinct range of compositions (Luque *et al.* 2012).

protolith could be supplemented by graphite precipitated from volatile solutions containing CO_2, H_2O and CH_4 during metamorphism, which should be evident in heavier carbon isotope values (Huizenga & Touret, 2012; Luque *et al.* 2012). Data for 31 graphite mines and prospective deposits in rocks of Palaeoproterozoic age (Fig. 3; Table S3, in the Supplementary Material available online at https://doi.org/10.1017/S0016756821000583), from 15 countries distributed globally, are consistently in the range −15 to −37 ‰. This range indicates an origin exclusively from organic matter, and not enriched from a carbonate source during metamorphism. Two separate databases for Palaeoproterozoic kerogen (Krissansen-Totton *et al.* 2015; Havig *et al.* 2017) confirm that organic matter of this age had $\delta^{13}C$ −35 to −20 ‰. The graphite therefore represents the anomalous Palaeoproterozoic deposition of organic carbon. By contrast, several graphite deposits deposited from volatile CO_2-rich solutions in Precambrian granulites have a range of −18 to −5 ‰ (Vry *et al.* 1988; Huizenga & Touret, 2012; Luque *et al.* 2012; Buseck & Beyssac, 2014). There *are* examples of graphite in Palaeoproterozoic marbles (limestones) with relatively heavy compositions (e.g. Garde, 1979), in which the graphite must be at least partially derived from decarbonation. However, these are minor showings, which do not impact on our dataset of rich graphite deposits.

3.4. Mineralization

Large nickel (+Co–Cu–PGE) deposits occur in mafic–ultramafic cumulate bodies, many of which were intruded through Palaeoproterozoic graphitic rocks (Hoatson *et al.* 2006). Assimilation of sulphur- and/or carbon-rich strata was critical to mineralization, as it caused sulphur saturation and sulphide precipitation in the magma. Assimilation is supported by sulphur isotope data (Ripley, 2014). The host rocks to Ni (+Co+Cu+PGE) intrusions have high S/C ratios typical of anoxic/euxinic sediments (Berner & Raiswell, 1983), and the high carbon contents are thus associated locally with abundant pyrite and pyrrhotite (Fig. 2). The sulphide-bearing graphitic hosts also contributed trace elements to the melt that promoted mineralization. For example, tellurium incorporated into pyrite in anoxic sediments became concentrated by assimilation into melts where it could precipitate PGE and gold tellurides (Peltonen, 1995; Samalens *et al.* 2017). Almost all of the largest post-Archaean nickel deposits are either of Palaeoproterozoic age, or they are younger but were intruded through and assimilated Palaeoproterozoic strata (Fig. 4). The assimilation of carbonaceous (and sulphidic) material is evidenced by xenoliths of metasediment, and by neoformed graphite crystallized from contaminated melt. Thus, graphite occurs in the super-large deposits formed at Voisey's Bay at 1.33 Ga, and Duluth at 1.1 Ga, and graphitic marble xenoliths occur in Jinchuan at 0.85 Ga, all following emplacement through graphitic Palaeoproterozoic rocks. At Duluth, the dependence of mineralization on assimilated carbon is especially evident from the distribution of ore bodies at the margin between the Duluth Complex intrusion and the host carbonaceous shales (Ripley *et al.* 2002; Ripley, 2014). Nickel and PGEs in these intrusions are commonly accompanied by cobalt, and some of the highest-tonnage bedrock cobalt resources are in intrusions which had assimilated Palaeoproterozoic graphitic sediment, including the younger intrusions at Voisey's Bay and Duluth (Slack *et al.* 2017) (Fig. 4). Unconformity-hosted deposits are the biggest producers of uranium ores. The highest-yielding deposits, in Canada and Australia, occur at unconformities between a Mesoproterozoic cover succession and a Palaeoproterozoic substrate. The substrate is consistently graphitic, especially in shear zones, and the graphite is attributed a role as a reductant and locus of high heat flow (Jefferson *et al.* 2007) or source of reducing methane (Branquet *et al.* 2019), although there is debate about whether the graphite is essential or not. While the Palaeoproterozoic graphite is 1.8 Ga or older, the uranium mineralization which it influenced may be substantially younger. Deposits in Canada and Australia were first mineralized at 1.59 Ga and 1.68 Ga respectively, but were reactivated at intervals

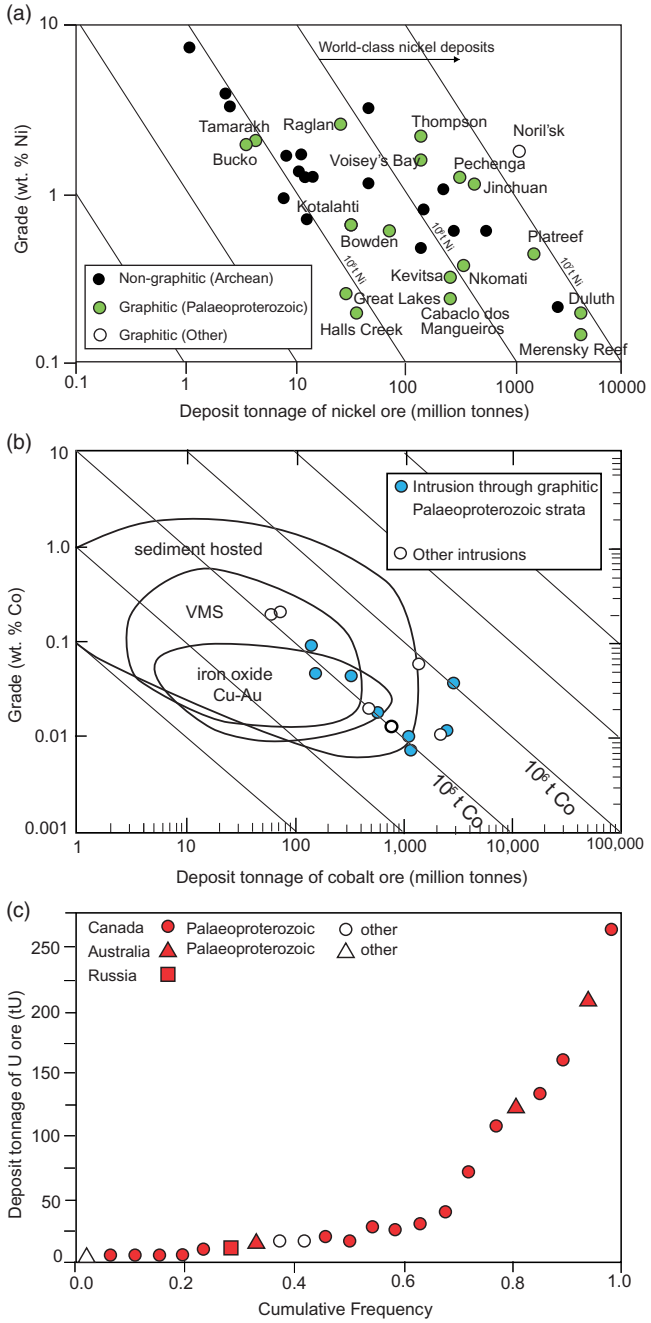

Fig. 4. (Colour online) High metal tonnages from mineralized intrusions and unconformities associated with Palaeoproterozoic graphitic hosts. (a) Nickel tonnages for largest deposits, modified from Hoatson *et al.* (2006), excluding impact-related Sudbury deposit. All non-Archaean deposits were intruded into carbonaceous rocks, and almost all into Palaeoproterozoic carbonaceous hosts. (b) Cobalt tonnages for largest deposit types in bedrock, omitting laterite and seafloor (Slack *et al.* 2017). Individual intrusions through Palaeoproterozoic carbonaceous hosts identified. (c) Unconformity-related uranium ore systems, expressed as cumulative mass of the 23 largest systems (IAEA, 2018), showing 97.5 % are associated with Palaeoproterozoic graphite.

up to the Phanerozoic (Jefferson *et al.* 2007). Elsewhere, graphite-bearing strata of Palaeoproterozoic age were mineralized over a billion-year period at 1.4 Ga in European Russia (IAEA, 2018), 1.23 Ga in the Russian Pacific (Goroshko & Gur'yanov, 2007), ~1.2 Ga in Rio Preto, Brazil (De Figueiredo Filho, 1984), 1.12 Ga in Shillong, India (Awati *et al.* 1995), and 0.8 Ga in Kintyre, Western Australia (IAEA, 2018). Of the 23 largest unconformity-related uranium ore systems, the largest 13, and 20 of the 23, are associated with Palaeoproterozoic graphite (Fig. 4), accounting for 97.5 % of the total tonnage (IAEA, 2018). Despite models in which the graphite is not essential to mineralization (Jefferson *et al.* 2007), this represents a very high proportion. In addition to uranium, some of these unconformity-related deposits also yield platinum group elements, gold, selenium and tellurium (Davidson & Large, 1994).

In summary, the ages of the ore deposits show that both the cumulate-hosted nickel and unconformity-related uranium mineralization occur 200 and more million years after deposition of the graphite (Fig. 5), i.e. the Palaeoproterozoic graphite has a long-term metallogenic legacy.

4. Discussion

4.1. High carbon contents

The very high organic richness of Palaeoproterozoic black shales (Condie *et al.* 2001) is matched by the very high mean carbon contents and abundance of commercial graphite deposits of Palaeoproterozoic age. Critically, the high carbon accumulation during the Palaeoproterozoic coincided with a relatively high crustal preservation potential, related to supercontinent assembly (Condie *et al.* 2001; Condie, 2014), leading to the long-term survival and mineralizing legacy of the Palaeoproterozoic carbon reservoir. The black shale data are derived from a geographically limited region (Australia, North America, Russia), but the graphite data represent several additional continents. Recent data include much information from Scandinavia, Ukraine, Brazil, India, China and several parts of Africa, and so confer much greater reliability as a global signature, and thus also support the global nature of the coupled Lomagundi–Jatuli and Shunga events.

The carbon isotope data for Palaeoproterozoic graphite, indicating an origin in sedimentary organic matter, link the graphite to the host sequences. In many cases, the graphitic beds have a bedding-parallel form that suggests that they represent layers in the original succession, for example in Palaeoproterozoic successions in South Australia (Keeling, 2017) and North Norway (Gautneb *et al.* 2020). The graphite commonly occurs in close proximity to non-commercial, but nonetheless highly graphitic, beds that are unequivocally metasediments. However, several lines of evidence indicate that the graphite beds were modified from the deposited beds. The graphite is commonly replacive, i.e. graphite overprinted other minerals, and graphite shows structurally-controlled thickening such as in fold hinges (e.g. Gautneb *et al.* 2020). Furthermore, ore graphite can be less crystallographically ordered than graphite in the background succession, as measured by Raman spectroscopy (e.g. Kříbek *et al.* 2015), showing that it was mobilized and/or modified. The distinction between high-sulphur graphitic metasediments and low-sulphur graphite deposits indicates a marked change in composition. Even in successions which contain sulphide ore mineralization in graphitic rocks, such as at Talvivaara, Finland (Kontinen & Hanski, 2015), and the Bhilwara/Aravalli supergroups, India (Mishra & Bernhardt, 2009), the commercial graphite prospects have low sulphur contents. This implies that carbon and sulphur had become fractionated during metamorphism, and is consistent with models in which graphitic sediments release large volumes of sulphur-rich fluids during metamorphism (Poulson & Ohmoto, 1989; Tomkins, 2010).

https://doi.org/10.1017/S0016756821000583

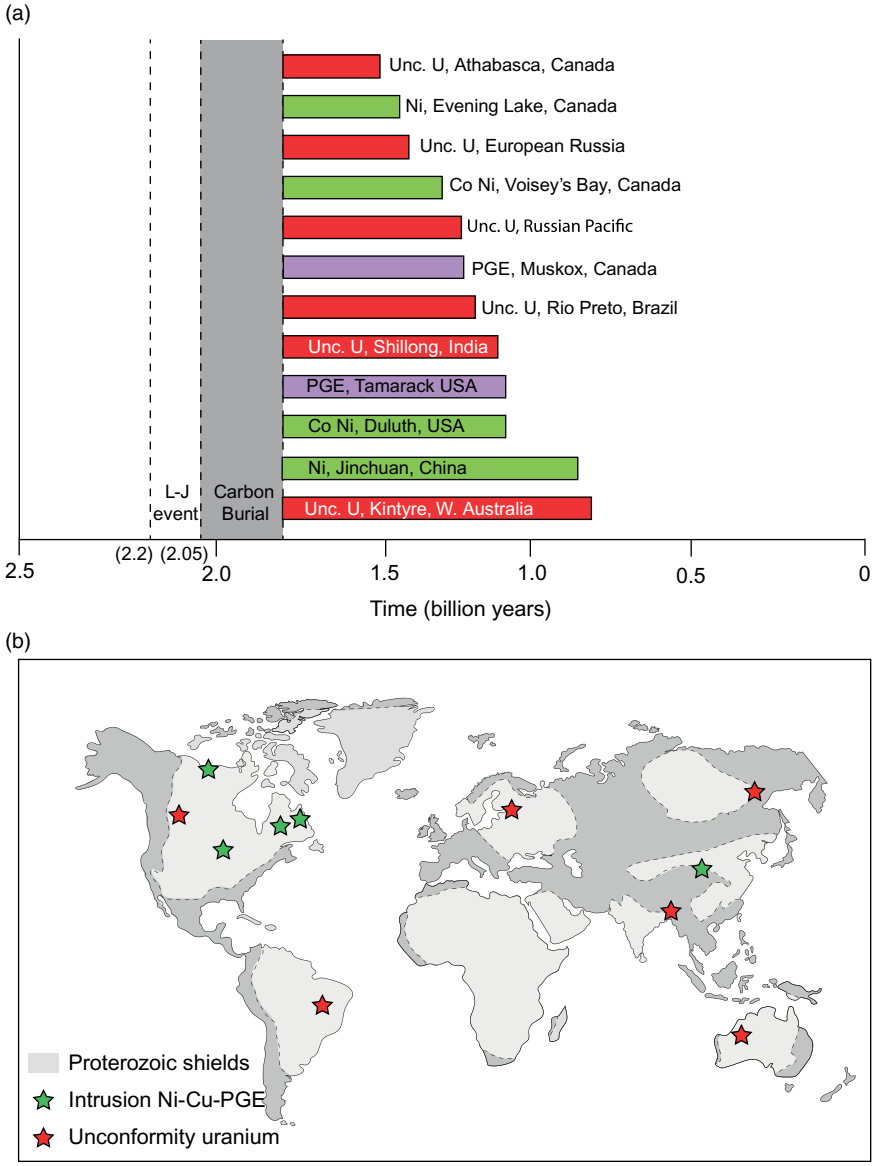

Fig. 5. (Colour online) Ore deposits genetically linked to Palaeoproterozoic graphite but formed at least 200 million years since graphite deposition. (a) Examples through time of ore deposits, in which the graphite influenced ore deposition for 2 billion years. (b) Global distribution of Proterozoic rocks, and examples of younger ore deposits associated with Palaeoproterozoic graphite beds.

4.2. Mineralization in Palaeoproterozoic rocks

Given the reductive properties of organic carbon, and the fundamental role of redox processes in metallogeny, a consequence of this episode of anomalous carbon burial was a step change in metal sequestration both during the Palaeoproterozoic and during subsequent geological history. The importance of the Palaeoproterozoic deposition of carbon to global metallogeny is evident by considering the diversity of metal ores precipitated, the tonnages of the ores, and the continued influence of the carbon through geologic time. Palaeoproterozoic rocks were extensively mineralized at the time of deposition, including iron formations and manganese mineralization both deposited from anoxic seawater and interbedded with graphitic rocks: about 65 % of global manganese reserves were deposited in the Palaeoproterozoic over 2.3–1.8 Ga (Havig *et al.* 2017; De Putter *et al.* 2018). However, a legacy of continued long-term mineralization was conferred by the physico-chemical nature of the graphitic beds. Firstly, the highly ductile nature of the graphite made it a focus for deformation and in particular the formation of shear zones, which channelled younger mineralizing fluids. Secondly, the conductive nature of the graphite may have engendered heat flow anomalies that caused fluid circulation. Thirdly, the reductive power of concentrated organic carbon made the graphite a chemical trap to pull metals out of solution. Fourthly, the carbon could be consumed in chemical reactions that precipitated metals. Fifthly, graphitic sediments are commonly sulphidic, as expected in marine shales, and sulphides co-precipitate trace elements during early diagenesis. These properties allowed a wide range of ores, involving different metals, to precipitate in Palaeoproterozoic graphitic rocks (Pirajno *et al.* 2003; Jefferson *et al.* 2007; Williams, 2007).

The distributions of the deposit types through time have different controlling factors. The uranium in unconformity-hosted deposits was derived particularly from the erosion of granites aged from Archaean to Mesoproterozoic. This uranium became

https://doi.org/10.1017/S0016756821000583

available before younger episodes of carbon precipitation and so is preferentially associated with crust rich in Palaeoproterozoic carbon. In the case of Ni–Co–Cu–PGE, even where the host intrusion is much younger than Palaeoproterozoic, where the intrusion cuts through the Palaeoproterozoic it may host ores formed by assimilation of Palaeoproterozoic graphite and sulphide. The high preservation potential of Palaeoproterozoic strata (Condie *et al.* 2001; Condie, 2014) has contributed to a dominance of country rocks of this age.

4.3. Mineral exploration

Much mineralization occurs in Archaean and Palaeoproterozoic rocks (Groves *et al.* 2005). This was followed by the so-called 'boring billion' period (1.8 to 0.8 Ga) when a combination of lower crustal growth and low preservation potential limit the mineralization record. Consequently, ore exploration occurs especially in Canada, Brazil, Australia, Scandinavia and North China, where much bedrock is Archaean and (Palaeo)proterozoic. Mineral exploration in these rocks has emphasized the importance of Palaeoproterozoic graphite. Fundamentally, graphitic rocks have guided the search for unconformity-related uranium in many countries (IAEA, 2018) and thus graphite has become an exploration target.

Exploration for several types of ore deposit makes use of the high electrical conductivity of the graphite. This allows the search for, and delineation of, individual ore deposits in the subsurface, for example deposits of unconformity-related uranium (Tuncer *et al.* 2006). However, graphite in Palaeoproterozoic successions is so abundant that it can be detected by geophysical techniques at the basin scale (Boerner *et al.* 1996; Zhamaletdinov, 1996; Lindsay *et al.* 2018). This abundance is not evident in rocks of younger ages, and the data evidences a substantial critical reservoir of graphite of Palaeoproterozoic age.

The strong link between metal ores and Palaeoproterozoic graphite is evident in frontier exploration areas where individual mining companies explore for both graphite and metals in adjoining or overlapping licences, including in Canada, Scandinavia, Africa and Australia (Table S4, in the Supplementary Material available online at https://doi.org/10.1017/S0016756821000583). Both ore types are essential to future, environmentally sensitive technologies (Gautneb *et al.* 2019). Most commonly, companies target both graphite and nickel ores, but graphite is also sought along with copper, uranium, gold and iron. This recent trend in exploration is likely to lead to discoveries which further demonstrate the strong link between Palaeoproterozoic graphite and metalliferous mineralization.

5. Conclusions: unique importance of Palaeoproterozoic carbon

The abundance of the world's largest graphite deposits that are of Palaeoproterozoic age supports previous inferences that the Palaeoproterozoic was a period of anomalously high carbon burial. The high S/C ratios for many Palaeoproterozoic shales show that, in addition to carbon, this was a period of high sulphide burial. The combined carbon and sulphur conveyed a reductive character to the sediments which gave them exceptional mineralizing potential.

Criteria for assessing the importance of Palaeoproterozoic carbon to mineralization, i.e. diversity of ores, tonnages of ores, and longevity of influence, all indicate a unique role for Palaeoproterozoic carbon in Earth's geological history. While there were episodes of deposition of single metals with greater tonnage, such as Archaean banded iron formations, longevity in the Palaeoproterozoic rocks was unequalled. The Palaeoproterozoic deposition of carbonaceous sediment had a greater control on the long-term metallogeny of the planet than any other depositional episode in the planet's history.

Declaration of Interest. The authors declare none.

Acknowledgements. This project is in support of the Natural Environment Research Council SoS (Security of Supply of Critical Elements) programme, under Grant NE/M010953/1. C Taylor, J Johnston and J Bowie provided skilled technical help. We are most grateful to H Gautneb and E Lynch for valuable review.

Supplementary material. To view supplementary material for this article, please visit https://doi.org/10.1017/S0016756821000583.

References

Andrews MS and Ripley EM (1989) Mass transfer and sulfur fixation in the contact aureole of the Duluth Complex, Dunka Road Cu-Ni deposit, Minnesota. *Canadian Mineralogist* **27**, 293–310.

Awati AB, Harikrishnan T, Sinha RM, Gupta KR and Gupta RK (1995) The Proterozoic Shillong Basin of North East India: conceptual model for hosting unconformity related uranium mineralization. *Exploration and Research for Atomic Minerals* **8**, 141–54.

Berner RA and Raiswell R (1983) Burial of organic carbon and pyrite sulfur in sediments over Phanerozoic time: a new theory. *Geochimica et Cosmochimica Acta* **47**, 855–62. doi: 10.1016/0016-7037(83)90151-5.

Boerner DE, Kurtz RD and Craven JA (1996) Electrical conductivity and Paleo-Proterozoic foredeeps. *Journal of Geophysical Research* **101**, 13775–791. doi: 10.1029/96JB00171.

Branquet Y, Boulvais P, Mercadier J, Ledru P and Khairallah C (2019) Methaniferous active faults and seismic cycle in the genesis of the Athabasca giant U deposits: conceptual and numerical investigation. In*15th SGA Biennial Meeting, Glasgow, 27–30 August 2019, Abstract volume 1*, pp. 52–5. Society for Geology Applied to Mineral Deposits.

Buseck PR and Beyssac O (2014) From organic matter to graphite: graphitization. *Elements* **10**, 421–6. doi:10.2113/gselements.10.6.421.

Chelgani SC, Rudolph M, Kratzsch R, Sandmann D and Gutzmer J (2016) A review of graphite beneficiation techniques. *Mineral Processing and Extractive Metallurgy Review* **37**, 58–68.

Condie KC (2014) Growth of continental crust: a balance between preservation and recycling. *Mineralogical Magazine* **78**, 623–37. doi: 10.1180/minmag.2014.078.3.11.

Condie KC, Des Marais DJ and Abbott D (2001) Precambrian superplumes and supercontinents: a record in black shales, carbon isotopes, and paleoclimates? *Precambrian Research* **106**, 239–60. doi: 10.1016/S0301-9268(00)00097-8.

Davidson GJ and Large RR (1994) Gold metallogeny and the copper-gold association of the Australian Proterozoic. *Mineralium Deposita* **29**, 208–23. doi: 10.1007/BF00206864.

De Figueiredo Filho PM (1984) The Rio Preto uranium occurrences. In *Proterozoic Unconformity and Stratabound Uranium Deposits* (ed. J Ferguson), pp. 313–23. Vienna: International Atomic Energy Agency. TECDOC-315 .

De Putter T, Liégeois J-P, Dewaele S, Cailteux J, Boyce A and Mees F (2018) Paleoproterozoic manganese and base metals deposits at Kisenge-Kamata (Katanga, D.R. Congo). *Ore Geology Reviews* **96**, 181–200doi: 10.1016/j.oregeorev.2018.04.015.

Garde AA (1979) Strontium geochemistry and carbon and oxygen isotopic compositions of Lower Proterozoic dolomite and calcite marbles from the Marmorilik Formation, West Greenland. *Precambrian Research* **8**, 183–99.

Gautneb H, Knežević J, Gloaguen E, Melleton J, Gourcerol B and Törmänen T (2019) Occurrences of energy critical elements; lithium – cobalt and graphite in Europe, a preliminary overview. In *Proceedings of the 15th SGA*

Biennial Meeting, 27–30 August 2019, Glasgow, pp. 1784–7. Society for Geology Applied to Mineral Deposits.

Gautneb H, Rønning JS, Engvik AK, Henderson IHC, Larsen BE, Solberg JK, Ofstad F, Gellein J, Elvebakk H and Davidsen B (2020) The graphite occurrences of northern Norway, a review of geology, geophysics, and resources. *Minerals* **10**, 626. doi: 10.3390/min10070626.

Goroshko MV and Gur'yanov VA (2007) Ore mineralization related to the zone of the Pre-Riphean structural-stratigraphic unconformity and Lower Riphean platform cover of the Uchur-Maya Depression, the Southeastern Siberian Platform. *Russian Journal of Pacific Geology* **1**, 586–601. doi: 10.1134/S1819714007060073.

Groves DI, Vielreicher RM, Goldfarb RJ and Condie KC (2005) Controls on the heterogeneous distribution of mineral deposits through time. In *Mineral Deposits and Earth Evolution* (eds I McDonald, AJ Boyce, IB Butler, RJ Herrington and DA Polya), pp. 71–101. Geological Society of London, Special Publication no. 248. doi: 10.1144/GSL.SP.2005.248.01.04.

Havig JR, Hamilton TL, Bachan A and Kump LR (2017) Sulfur and carbon isotopic evidence for metabolic pathway evolution and a four-stepped Earth system progression across the Archean and the Paleoproterozoic. *Earth-Science Reviews* **174**, 1–21. doi: 10.1016/j.earscirev.2017.06.014.

Hoatson DM, Jaireth S and Jaques AL (2006) Nickel sulfide deposits in Australia: characteristics, resources, and potential. *Ore Geology Reviews* **29**, 177–241. doi: 10.1016/j.oregeorev.2006.05.002.

Huizenga JM and Touret JLR (2012) Granulites, CO_2 and graphite. *Gondwana Research* **22**, 799–809. doi: 10.1016/j.gr.2012.03.007.

Huyck HLO (1990) When is a metalliferous black shale not a black shale? In*Metalliferous Black Shales and Related Ore Deposits – Proceedings, 1989 Working Group Meeting, International Geological Correlation Program, Project 254* (eds RI Grauch and HLO Huyck), pp. 42–56. Reston, Virginia: US Geological Survey Circular 1058.

International Atomic Energy Agency (IAEA) (2018) *Unconformity-related Uranium Deposits*. Vienna: International Atomic Energy Agency. IAEA-TECDOC 1857.

Jefferson CW, Thomas DJ, Gandhi SS, Ramaekers P, Delaney G, Brisbin D, Cutts C, Quirt D, Portella P and Olson RA (2007) Unconformity-associated uranium deposits of the Athabasca Basin, Saskatchewan and Alberta. In *Mineral Deposits of Canada: A Synthesis of Major Deposit-Types, District Metallogeny, the Evolution of Geological Provinces, and Exploration Methods* (ed. WD Goodfellow), pp. 273–305. St John's: Geological Association of Canada, Mineral Deposits Division, Special Publication No. 5. doi: 10.2113/gsecongeo.102.7.1355.

Keeling J (2017) Graphite: properties, uses and South Australian resources. *MESA Journal* **84**, 28–41.

Kontinen A and Hanski E (2015) The Talvivaara black shale-hosted Ni-Zn-Cu-Co deposit in Eastern Finland. In *Mineral Deposits of Finland* (eds WD Maier, R Lahtinen and H O'Brien), pp. 557–612. Amsterdam: Elsevier.

Kríbek B, Sýkorová I, Machovič V, Knésl I, Laufek F and Zachariáš J (2015) The origin and hydrothermal mobilization of carbonaceous matter associated with Paleoproterozoic orogenic-type gold deposits of West Africa. *Precambrian Research* **270**, 300–17.

Krissansen-Totton J, Buick R and Catling DC (2015) A statistical analysis of the carbon isotope record from the Archean to Phanerozoic and implications for the rise of oxygen. *American Journal of Science* **315**, 275–316. doi: 10.2475/04.2015.01.

Lindsay MD, Spratt J, Occhipinti SA, Aitken ARA, Dentith MC, Hollis JA and Tyler IM (2018) Identifying mineral prospectivity using 3D magnetotelluric, potential field and geological data in the east Kimberley, Australia. In *Characterization of Ore-Forming Systems from Geological, Geochemical and Geophysical Studies* (ed. K Gessner, TG Blenkinsop and P Sorjonen-Ward), pp. 247–68. Geological Society of London, Special Publication no. 453. doi: 10.1144/SP453.8.

Lu XJ and Forssberg E (2002) Preparation of high-purity and low-sulphur graphite from Woxna fine graphite concentrate by alkali roasting. *Minerals Engineering* **15**, 755–7.

Luque FJ, Crespo-Feo E, Barrenechea JF and Ortega L (2012) Carbon isotopes of graphite: implications on fluid history. *Geoscience Frontiers* **3**, 197–207. doi: 10.1016/j.gsf.2011.11.006.

Martin AP, Prave AR, Condon DJ, Lepland A, Fallick AE, Romashkin AE, Medvedev PV and Rychanchik DV (2015) Multiple Palaeoproterozoic carbon burial episodes and excursions. *Earth and Planetary Science Letters* **424**, 226–36. doi: 10.1016/j.epsl.2015.05.023.

Melezhik V, Fallick AE, Martin AP, Condon D, Kump L, Brasier AT and Salminen P (2013) The Palaeoproterozoic perturbation of the global carbon cycle: the Lomagundi-Jatuli Isotopic Event. In *Reading the Archive of Earth's Oxygenation, vol. 3: Global Events and the Fennoscandian Arctic Russia – Drilling Early Earth Project*, pp. 1111–50. Berlin: Springer-Verlag. doi: 10.1007/978-3-642-29670-3_3.

Melezhik VA, Grinenko LN and Fallick AE (1998) 2000-Ma sulphide concretions from the 'Productive' Formation of the Pechenga Greenstone Belt, NW Russia: genetic history based on morphological and isotopic evidence. *Chemical Geology* **148**, 61–94. doi: 10.1016/S0009-2541(98)00021-7.

Melezhik VA, Huhma H, Condon DJ, Fallick AE and Whitehouse MJ (2007) Temporal constraints on the Paleoproterozoic Lomagundi-Jatuli carbon isotope event. *Geology* **35**, 655–8. doi: 10.1130/G23764A.1.

Mishra B and Bernhardt H-J (2009) Metamorphism, graphite crystallinity, and sulphide anatexis of the Rampura-Agucha massive sulphide deposit, northwestern India. *Mineralium Deposita* **44**, 183–204.

Paiste K, Pellerin A, Zerkle AL, Kirsimäe K, Prave T, Romashkin AE and Lepland A (2020) The pyrite multiple sulfur isotope record of the 1.98 Ga Zaonega Formation: evidence for biogeochemical sulfur cycling in a semi-restricted basin *Earth and Planetary Science Letters* **534**, 116092. doi: 10.1016/j.epsl.2020.116092.

Partin CA, Bekker A, Planavsky NJ and Lyons TW (2015) Euxinic conditions recorded in the ca. 1.93 Ga Bravo Lake Formation, Nunavut (Canada): implications for oceanic redox evolution. *Chemical Geology* **417**, 148–62. doi: 10.1016/j.chemgeo.2015.09.004.

Pascal M, Ansdell KM and Annesley IR (2015) Graphite-bearing and graphite-depleted basement rocks in the Dufferin Lake Zone, South-central Athabasca Basin, Saskatchewan. In *Targeted Geoscience Initiative 4: Unconformity-Related Uranium Systems* (eds EG Potter and DM Wright), pp. 83–92. St John's: Geological Survey of Canada, Open File 7791. doi: 10.4095/295776.

Peltonen P (1995) Magma-country rock interaction and the genesis of Ni-Cu deposits in the Vammala Nickel Belt, SW Finland. *Mineralogy and Petrology* **52**, 1–24. doi: 10.1007/BF01163124.

Pirajno F, Thomassen B and Dawes PR (2003) Copper-gold occurrences in the Palaeoproterozoic Inglefield mobile belt, northwest Greenland: a new mineralisation style? *Ore Geology Reviews* **22**, 225–49. doi: 10.1016/S0169-1368(02)00143-9.

Poulson SR and Ohmoto H (1989) Devolatilization equilibria in graphite-pyrite-pyrrhotite bearing pelites with application to magma-pelite interaction. *Contributions to Mineralogy and Petrology* **101**, 418–25.

Raiswell R and Berner RA (1987) Organic carbon losses during burial and thermal maturation of normal marine shales. *Geology* **15**, 853–6.

Ripley EM (2014) Ni-Cu-PGE mineralization in the Partridge River, South Kawishiwi, and Eagle intrusions: a review of contrasting styles of sulphide-rich occurrences in the Midcontinent Rift System. *Economic Geology* **109**, 309–24. doi: 10.2113/econgeo.109.2.309.

Ripley EM, Li C and Shin D (2002) Paragneiss assimilation in the genesis of magmatic Ni-Cu-Co sulfide mineralization at Voisey's Bay, Labrador: $\delta^{34}S$, $\delta^{13}C$, and Se/S evidence. *Economic Geology* **97**, 1307–18. doi: 10.2113/gsecongeo.97.6.1307.

Robinson GR, Hammarstrom JM and Olson DW (2017) Graphite.. *United States Geological Survey Professional Paper* 1802-J. doi:10.3133/pp1802J.

Samalens N, Barnes S and Sawyer EW (2017) The role of black shales as a source of sulfur and semimetals in magmatic nickel-copper deposits: example from the Partridge River Intrusion, Duluth Complex, Minnesota, USA. *Ore Geology Reviews* **81**, 173–87. doi: 10.1016/j.oregeorev.2016.09.030.

Slack JF, Kimball BE and Shedd KB (2017) Cobalt. *United States Geological Survey Professional Paper* 1802-F. doi: 10.3133/pp1802F.

Strauss H, Melezhik VA, Lepland A, Fallick AE, Hanski EJ, Filippov MM, Deines YE, Illing CJ, Črne AE and Brasier AT (2013) Enhanced accumulation of organic matter: the Shunga Event. In *Reading the Archive of Earth's*

Oxygenation (eds V Melezhik, AR Prave, EJ Hanski, AE Fallick, A Lepland, LR Kump and H Strauss), pp. 1195–1273. Berlin: Springer.

Tomkins AG (2010) Windows of metamorphic sulfur liberation in the crust: implications for gold deposit genesis. *Geochimica et Cosmochimica* **74**, 3246–59.

Tuncer V, Unsworth MJ, Siripunvaraporn W and Craven JA (2006) Exploration for unconformity-type uranium deposits with audiomagnetotelluric data: a case study from the McArthur River mine, Saskatchewan, Canada. *Geophysics* **71**, B201–9.

Vry J, Brown PE, Valley JW and Morrison J (1988) Constraints on granulite genesis from carbon isotope compositions of cordierite and graphite. *Nature* **332**, 66–8. doi: 10.1038/332066a0.

Williams NC (2007) The role of decarbonization and structure in the Callie gold deposit, Tanami Region of northern Australia. *Mineralium Deposita* **42**, 65–87. doi: 10.1007/s00126-006-0096-0.

Zhamaletdinov AA (1996) Graphite in the Earth's Crust and electrical conductivity anomalies. *Izvestiya Physics Solid Earth* **32**, 272–88.

https://doi.org/10.1017/S0016756821000583